RSC Advances

ROYAL SOCIETY OF CHEMISTRY

www.rsc.org/advances

RSC Advances

ARTICLE

The effect of the octan-3-yloxy and the octan-2-yloxy chiral moiety on the mesomorphic properties in ferroelectric liquid crystals

Received 00th January 20xx,
Accepted 00th January 20xx

DOI: 10.1039/x0xx00000x

www.rsc.org/

Dorota Węgłowska, Paweł Perkowski, Wiktor Piecek, Mateusz Mrukiewicz and Roman Dąbrowski

New mesogenic compounds exhibiting unique, so called orthoconic behavior at the synclinic smectic SmC* phase have been obtained. Newly synthesized compounds belong to two chiral homologous series of 4'-[ω-(2,2,3,3,4,4,4-heptafluorobutoxy)alkoxy]biphenyl-4-yl 4-(octan-2-yloxy)benzoates and 4'-[ω-(butoxy)alkoxy]biphenyl-4-yl 4-(octan-3-yloxy)benzoates. Their mesogenic behavior has been studied and their phase transition temperatures as well as enthalpies have been evaluated using polarizing optical microscope, differential scanning calorimetry and dielectric spectroscopy technique. The tilt angle, the spontanoues polarisation as well as the helical pitch of the compounds have been studied at the full temperature domain. The compounds with 4'-ω-(2,2,3,3,4,4,4-heptafluorobutoxy)alkoxy terminal chain exhibit polar smectic C* phase. The analogous compound with 4'-ω-(butoxy)alkoxy achiral terminal chain and octan-2-yloxy chiral part exhibits Iso-N*-SmC* phase sequence, while that one with octan-3-yloxy chiral part does not exhibit mesogenic behavior. The compounds with the octan-3-yloxy chiral part exhibit much lower melting points than those with the octan-2-yloxy chiral part. The clearing points of new compounds decrease with the increase of the length of the oligomethylene spacer chain. Dielectric studies confirmed the presence of SmC* and N* phases. The tilt angles measured in the SmC* phase reveal extremally high values at saturation approaching 45°. The values of the spontaneous polarization for all investigated compounds are as high as 89.5nC/cm^2. The lenght of the helical pitch for different compounds is changing from 460.7nm to 1367.7nm.

1 Introduction

Since N. A. Clark and S. T. Lagerwall have demonstrated in 1980[1] the fast switching electro-optical effects based on surface stabilized ferroelectric liquid crystals (SSFLCs), ferroelectric smectic liquid crystals (FLCs) have been extensively studied[2-9]. The main problem in the use of FLCs in photonic applications is the difficulty of obtaining the homogenous and permanent structure (resistant to mechanical shock) of the smectic layers inside the liquid crystal cell. Mechanical shock resistance of FLCs can be increased by stabilizing the smectic layer with a polymer network[10].

In 1995 Fukuda mentioned for the first time the *V*-shape electro-optic response[11] exhibiting electro-optical characteristic similar to that one observed for nematic liquid crystals, which is potential to become a very promising technology in photonic applications. The electro-optical effect in ferroelectric liquid crystal stabilized by polymer network (PSV) exhibiting *V*-shape switching was developed by Japanese company Dainippon Ink and Chemicals. FLCs working in PSV mode exhibit short switching times (100-200μs[12]) and high contrast ratio. In addition, they require low applied voltage (<10V). The most preferred compounds for the PSV effect should exhibit high tilt angle (near 45°) and the phase sequence: Iso-N*-SmA*-SmC* (INAC phase sequence). In the PSV effect the length of the helical pitch of the FLC plays no role.

In the deformed helix ferroelectric effect (DHF)[13-16,24] the helix axis is parallel to the substrates plane. This electrooptical effect is observed while the helical structure is affected with a weak electric field *E* (which is less than the critical field E_C of the helix unwinding). The critical electric field E_C and the switching time τ are given by the equations: (1) and (2):

$$\tau = \frac{\gamma_\varphi p^2}{K 4\pi^2} \quad (1) \qquad \text{and} \qquad E_C = \frac{\pi^4}{4}\frac{K}{P_S p^2} \quad (2)$$

where: γ_φ is rotation viscosity, p is helical pitch, K is elastic constant and P_s is spontaneous polarization.

[a] Faculty of Advanced Technologies and Chemistry, Military University of Technology, 2 Kaliskiego Str., 00-908 Warsaw 49, Poland. Email: dorota.weglowska@wat.edu.pl

† Electronic Supplementary Information (ESI) available. See DOI: 10.1039/x0xx00000x

The electric field value required for the helix deformation and the deviation of the optical axis of the FLC slab in plane of the measuring cell is low[22].

The helical pitch p of the FLC structure within a cell prepared for observation of the DHF effect is much smaller than the cell gap d ($p<<d$), so that the structure can be considered as free from boundary surface induced distortions[17]. In consequence, the helix becomes wound within the cell[18] in contrast to the SSFLC effect, where the surface induces unwinding of the helix and it requires the helical pitch of the FLC to be longer than the cell thickness. The director of the ferroelectric liquid crystal structure inside the cell in DHF mode is arrangement in the similar way as in SSFLC effect, but with such a difference that the helix of FLC is not unwound. The DHF mode has been regarded very promising for display and photonic applications. When an electric field is applied lower than critical electric E_C field between the two substrate plates it couples to the spontaneous polarization in each molecular layer. The helical structure become deformed and then fully untwisted for the electric filed higher than critical field E_C. The helical pitch at the DHF effect should be preferably short (p<1μm) and the tilt angle should be relatively large (θ>30°)[18,19]. At the DHF mode, the light transmission T of the cells, placed between crossed polarizers (see Figure 1) is described by the relationship (3)[20]:

$$T = \sin^2 2[\beta \pm \Delta\alpha] \cdot \sin^2 \frac{\pi d \ \Delta n_{eff}}{\lambda} \qquad (3)$$

where: β is an angle between the polarizer and helix axis x of the ferroelectric phase; $\Delta\alpha$ is the shift of helical axis due to electric field; Δn_{eff} is an effective birefringence and λ is the wavelength.

Non-sensitive to the polarity of the driving voltage an electro-optical response is obtain for geometry with β=0[21]. Maximum light transmission under this condition occurs if:

$$\Delta\alpha = \pi/4 \qquad (4) \qquad \text{and} \qquad \frac{\pi d \ \Delta n_{eff}}{\lambda} = \pi/2 \qquad (5)$$

so, the tilt angle θ of the FLC should be close to 45° (π/4) for providing of maximum light transmission at β=0[20,22]:

$$\Delta\alpha \leq \theta \qquad (6)$$

The helical configuration at the DHF mode exhibits wide range of unique optical properties such as the circularly polarized Bragg type reflection and the huge optical rotatory dispersion. Switching time of the DHF is short, less than 100μs, at very low applied voltage (1V/μm). The switching curve is hysteresis-free V-shape and near independent upon the frequency of the applied voltage in a broad frequency range (10Hz – 4kHz).

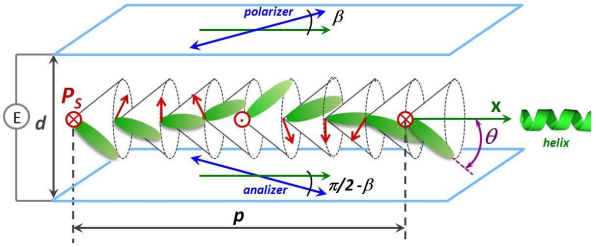

Figure 1. The schematic drawing of the DHF mode in the planar cell.

Above features make FLCs working at DHF mode very useful for tuneable filters, thermography, electrically tuneable optical diodes[23], biosensors[24], voltage sensors[25-28], spatial light modulators[29-32], real-time multi-point measurements, under water sonar array systems[33-35] such as fiber optic hydrophone array system that could be used for underwater acoustic surveillance applications (e.g. military, counter terrorist and customs authorities in protecting ports and harbours) and many other various applications[36].

For mentioned above electro-optic effect ferroelectric liquid crystals having low melting point, broad temperature range of SmC* phase, high tilt angle, high spontaneous polarization and short helical pitch are especially promising. The assortment of high tilted FLCs is still limited.

There is a strong relationship between the molecular structure of the FLCs and its mesomorphic and electro-optical properties[29-30]. Even a small change of the molecular structure influences on its properties[39-41]. The first family of highly tilted FLCs described T. Inukai *et al.*[42] (see formula **I**):

I

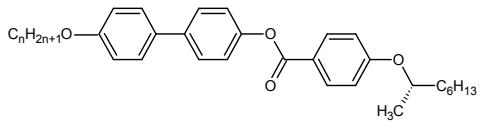

n	Cr		SmC*		N		Iso	θ [°]
7	•	88.2	•	93.5	•	120.4	•	45
8	•	78.3	•	98.4	•	121.1	•	45
9	•	79.1	•	101.0	•	117.1	•	45

In compounds **I** the molecular director is tilted in respect to the smectic layers normal at the angle of 45°. They exhibit a phase sequence: Iso-N*-SmC*. With the elongation of the alkoxy chain $C_nH_{2n+1}O$- the stability of the SmC* phase increases and the melting point of the compounds decreases. Compounds **I** synthesized by Inukai exhibit high melting points, what makes such compounds less useful for photonic applications.

In 2011 C. Liao *et al.*[43] synthesized compounds with a siloxane terminal chain exhibiting much lower melting points (compounds of formula **II**):

II

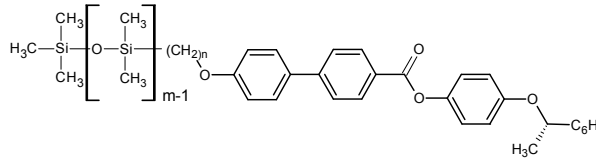

m	n	Cr		SmC*		Iso	θ[°]	τ[μs]
6	**2**	●	1.3	●	88.9	●	45	23
11	**3**	●	46.9	●	106.9	●	44	35

Switching times of such compounds are very short (less than 40μs), but the applied voltage is high (160V at the cell gap of 7.5μm). Such behaviour is ascribed to the presence of the bulky dimethylsiloxane group, which shows less flexibility and small number of conformational states than the alkyl chain compounds.

Continuing our previous studies[44-45] we have decided to synthesize two homologous series of new chiral esters with general formulae **III**:

III 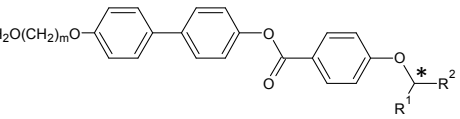

wherein: X=H or F; m=2-7; either: R^1=CH_3 and R^2= C_6H_{13} for (*S*)-(+)-octan-2-yloxy derivatives or R^1=C_2H_5 and R^2=C_5H_{11} for (*R*)-(-)-octan-3-yloxy derivatives.

These compounds are abbreviated 3XOmCk, where X is the hydrogen or fluorine atom at the achiral terminal chain, m is the length of the oligomethylene spacer between the rigid core and the first alkoxy group of the terminal chain and k is the number of carbon atoms in R^1 group at the chiral terminal chain. Either R^1 is a methyl group (k=1) and R^2 is an hexyl- group [obtained from of (*S*)-(+)-octan-2-ol; series nXOmC1] or R^1 is an ethyl group (k=2) and R^2 is an pentyl- group [obtained from (*R*)-(-)-octan-3-ol; series nXOmC2]. Temperatures and enthalpies of the phase transitions, tilt angle, spontaneous polarization as well as the helical pitch in the SmC* phase of homologues described above have been examined.

2 Experimental

2.1 Synthesis

The method of synthesis of final compounds 3XOmC2 [prepared from (*S*)-(+)-octan-3-ol] is shown in Scheme 1 and described in M. Sc. Thesis[46]. The preparative procedures of final compounds 3XOmC2 and 3XOmC1 [prepared from (*R*)-(-)-octan-2-ol] are presented in the ESI†. The preparative procedures of needed chiral phenol 8b [(*S*)-(+)-4'-hydroxybiphenyl-4-yl 4-(octan-3-yloxy)benzoate] has been presented in our earlier papers[44-45]. For the chiral functionalization (compounds 4a) the Mitsunobu etherification[47] has been used. During this reaction the configuration at the chiral carbon atom is inversed. This method was also used to coupling the chiral phenol (8a) with proper butoxyalkanol or 2,2,3,3,4,4,4-heptafluorobutoxy alkanol. The method of the synthesis of 2,2,3,3,4,4,4-heptafluorobutoxy alkanols described by P. Kula *et al.*[48]

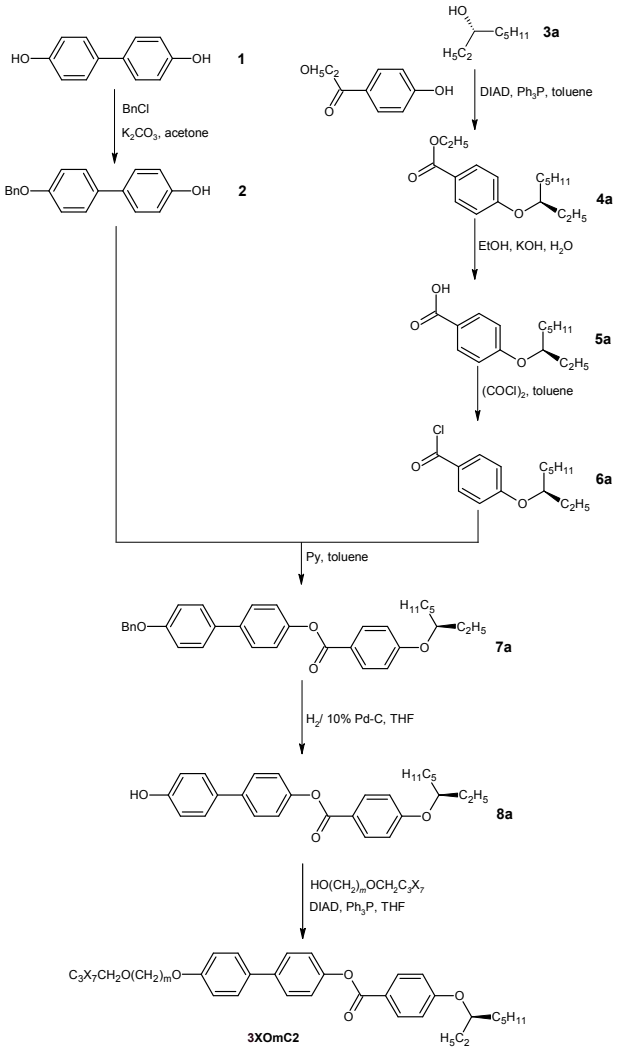

Scheme 1. The synthesis route of compounds 3XOmC2 (prepared from (*S*)-(+)-octan-3-ol).

The preparative procedures of final compounds 3XOmCk and their characterization by GC-MS, HPLC-MS methods and by ^{1}H and ^{1}C NMR spectroscopy are presented in the ESI.†

3 Results and discussion

3.1 Mesomorphic properties

Mesophases have been identified conventionally by observing textures using Olympus polarizing optical microscope (POM) with crossed polarizers and equipped with the Linkam TMSH 600 hot stage and the Linkam TMS 93 temperature controller. Phases have been additionally confirmed on the basis of results of the dielectric studies. The temperatures and enthalpies of the phase transition have been determined by a differential scanning calorimetry using DSC SETARAM 141 instrument with the scanning rate 2°C/min in both heating and cooling cycles. In Table 1 the temperatures and

the enthalpies of the phase transitions of compounds of series 3XOmCk are presented.

Table 1. The phase transition temperatures [°C] (upper row; onset point) and the enthalpies [kJ/mol] (lower row) of the members of the homologous series 3XOmCk from DSC measurements determined during heating (values given in the brackets were determined upon cooling).

Acr.	Cr2	Cr	SmX*	SmC*	N*	Iso
3FO2C1		• 96.0 *27.96*		• 132.4 *8.62*		•
3FO3C1	• 43.1 *3.91*	• 84.3 *25.93*		• 114.5 *6.58*		•
3FO4C1		• 82.2 *14.98*		• 135.6 *8.53*		•
3FO5C1		• 77.8 *37.01*		• 123.7 *7.03*		•
3FO6C1		• 70.8 *32.79*		• 129.2 *8.21*		•
3FO7C1	• 37.3 *8.93*	• 74.5 *33.13*		• 123.1 *7.71*		•
3HO3C1		• 74.3 *39.89*	• (55.7) *-0.71*	• (71.2) *-3.83*	• 83.1 *0.77*	•
3FO2C2		• 87.0 *24.83*		• 92.6 *5.40*		•
3FO3C2		• 73.7 *38.78*		• (72.4) *-3.75*		•
3FO5C2		• 49.6 *27.10*		• 75.6 *3.32*		•
3FO7C2		• 36.8 *16.44*		• 78.0 *3.55*		•
3HO3C2		• 40.1 *33.97*				•

Acr.-acronim

Compounds of fluorinated series 3FOmC1 and 3FOmC2 exhibit the SmC* phase only (with the direct SmC*-Iso transition). The members of the homologous series 3FOmC1 with m=5, 6 and 7 exhibit very high melting enthalpy (above 32kJ/mol). In case of the protonated analogues compound 3HO3C1 the nematic phase above and a more ordered tilted smectic phase below the synclinic SmC* phase have been observed upon cooling. Similar to Inukai compounds with the alkyl or alkoxy terminal chain the Iso-N*-SmC* phase sequence have here been observed. The melting points of compounds of the series 3FOmC1 decrease with the increase of the index m in the terminal achiral alkyl chain. An exception is compound 3FO7C1, which exhibits a little higher melting point than compound 3FO6C1. Members: 3FO3C1, 3FO5C1 and 3FO7C1 exhibit lower clearing point than members: 3FO2C1, 3FO4C1 and 3FO6C1, so the characteristic odd-even effect is observed[49]. In Figure 2 the effect of the number of carbon atoms m in the oligomethylene spacer on the melting and clearing points for the compounds 3FOmC1 is presented.

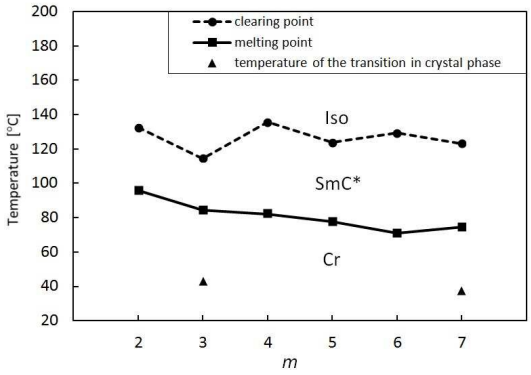

Figure 2. The effect of the number of carbon atoms in the oligomethylene spacer on the melting points (the Cr-SmC* transition) and clearing points (the SmC*-Iso transition) for the compounds 3FOmC1.

The fluorinated members of homologous series 3FOmC2, wherein m=2, 5 and 7 exhibit the enantiotropic SmC* phase accompanied with the direct SmC*-Iso transition, while the member wherein m=3 (compound 3FO3C2) exhibits the monotropic SmC* phase. Their clearing and the melting points are much lower. This is a typical behavior observed for the compounds with a larger branched chain (an ethyl- instead of a methyl- group). The melting points of compounds of the series 3FOmC2 decrease with the increase of the length of the oligomethylene spacer (index m). Compound 3FO7C2 exhibits the lowest melting point, 36.8°C only. For the protonated compound 3HO3C2 (no fluorine atom substituted) no mesophase is observed.

Compounds of series 3FOmC1 exhibit the focal-conic texture of the SmC* phase, while members of series 3FOmC2 forms strongly defected microscopic pattern of the SmC* with small domains, see Figure 3.

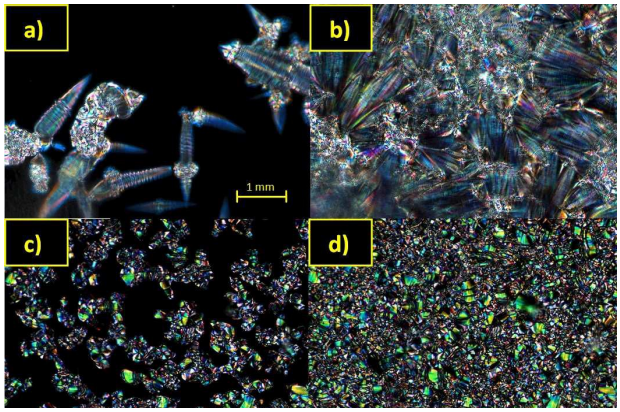

Figure 3. The micrograph of the textures observed during cooling for compounds: 3FO6C1: a) during the Iso-SmC* transition at 129.0°C, b) the SmC* phase at 90.2°C and 3FO5C2: c) during the Iso-SmC* transition at 75.5°C and d) the SmC* phase at 53.7°C.

3.2 Dielectric measurements

The measurements have been done by using a HP 4192A impedance analyzer and custom-made measuring cells[50]. A low-

resistivity ITO layer (10 Ω/□) has been used to avoid the high-frequency losses related to finite conductivity of ITO electrodes[51]. Short wires of a low-resistivity have been used for connection of the measuring cells to the impedance analyzer. Cells with the thickness of 5μm covered with polyimide SE130 as an aligning layer and antiparallel rubbed have been used. The cells were filled by capillary action at the isotropic phase, at the temperature close to the clearing point. Due to that the cell gap is small, applying a small value of AC voltage (0.5V) creates a large electric field *E*=100kV/m. For this reason measurements have been conducted at low (0.1V) measuring voltage applied. Such AC voltage is enough for the electric current response easy to interpret by the impedance analyzer. Additionally, such AC voltage creates electric field (*E*) which is far from a level producing nonlinear effects in liquid crystals. 0.1V electric voltage of AC measuring signal allows us to ignore nonlinearity in dielectric response. During measurements no bias (DC) voltage was applied. Measuring frequencies varied from 100Hz up to 10MHz. Temperature of the measuring cells has been controlled using a computer driven Linkam TMS 92 unit and a hot stage Linkam THMSE 600 at an accuracy of 0.1°C. During measurements cells were slowly cooled at a rate of 0.3°C/min.

In Figure 4 the real part ε′ of electric permittivity at six frequencies (0.1, 1, 10, 100kHz, 1 MHz and 10MHz) versus temperature for compound 3FO5C2, chosen as a typical member of fluorinated series, has been shown. At the frequency below 1kHz strong dispersion is observed. This dispersion is typical for the SmC* phase. It falls with the increase of the frequency. The observed mode can be interpreted as a Goldstone mode[52]. The Goldstone mode is a collective relaxation, which is related with the procession of tilted molecules around the helical axis observed in ferroelectric SmC* phase. It is the strongest mode observed in liquid crystals built from rod-like molecules. It is not Arrhenius-type relaxation. The relaxation frequency of Goldstone mode varies usually from 100Hz to 10kHz. Using our calculation procedure[53-54] the parameters of the Goldstone mode for four temperatures have been calculated. In Table 2 the results are shown. The dielectric strength $\delta\varepsilon$ for compound 3FO5C2 decreases with the temperature decrease. The same effect is observed for the relaxation frequency of the Goldstone mode. Due to the fact that in the investigated compound a direct nucleation of clusters at SmC* phase has been observed at the temperature of the phase transition from the isotropic liquid hence one cannot observe the soft mode[52]. One can see that the dielectric spectroscopy results confirm the phase sequences observed from the differential scanning calorimetry (DSC) measurements. Transitions observed at cooling cycle for compound 3FO5C2 are as follows: Iso 77.5°C SmC* 31.5°C Cr. The plot for the frequency of 10MHz is influenced by cell properties[53-54] due to resistivity of ITO electrodes. It means that ε′ values presented for 10MHz are slightly underestimated.

In Figure 5 the real part ε′ of electric permittivity at six frequencies (0.1, 1, 10, 100kHz, 1MHz and 10MHz) versus temperature for compound 3HO3C1 is shown. The plot for 10MHz is influenced by the properties of the measuring cell (cut-off frequency of the measuring cell), as it is for measurements of 3FO5C2. The observed dielectric spectrum confirms all phases observed by DSC method. The phase transition temperatures determined by the dielectric spectroscopy differ a little in comparison with the DSC results: Iso 84.5°C N* 72.5°C SmC* 55°C SmX 48.5°C Cr. In addition, more ordered smectic phase (SmX) with hindered dispersion below the SmC* phase is observed. The well defined Goldstone mode is observed too, while soft mode is not observed in dielectric response of 3HO3C1, due to the absence of the SmA* phase. The parameters of the Goldstone mode for two values of the temperature: 70 and 60°C were calculated. The results of these calculations are presented in Table 2.

Table 2. The parameters of the Goldstone mode (dielectric strength $\delta\varepsilon$, and the relaxation frequency f_R) for compounds: 3FO5C2 and 3HO3C1.

Acronim	Parameter	70°C	60°C	50°C	40°C
3FO5C2	$\delta\varepsilon$	52.2	44.2	40.6	28.5
	f_R	420 kHz	340 kHz	220 kHz	150 kHz
3HO3C1	$\delta\varepsilon$	12.4	11.2		
	f_R	2900 kHz	2020 kHz		

Dielectric strength $\delta\varepsilon$ exhibited by compound 3HO3C1 is four times smaller than in case of compound 3FO5C2 (at the same value of the temperature). It means that fluorine atoms can support stronger dielectric response of the Goldstone mode. The relaxation frequency of the Goldstone mode of compound 3HO3C1 is higher than in case of compound 3FO5C2, because 3FO5C2 molecule is much larger and heavier than 3HO3C1 molecule. Longer and larger object shows lower relaxation frequency than the shorter and the lighter ones.

In case of compound 3FO5C2 at the isotropic phase, near to the Iso-SmC* transition, the weak dispersion is observed, at high frequencies. It is worth to notice that it can be interpreted as a dielectric response of the molecular rotation around short molecular axis (S-mode)[55]. This S-mode is strongly temperature dependent. In the SmC* phase S-mode is hindered. Such mode should be easily detectable both in the isotropic and in the nematic phases, but molecule of compound 3HO3C1 are too light in comparison with the molecule of compound 3FO5C2 and hence the relaxation frequency of S-mode in compound 3HO3C1 is much higher than in compound 3FO5C2 and cannot be observed using our experimental setup (limited frequency measuring range).

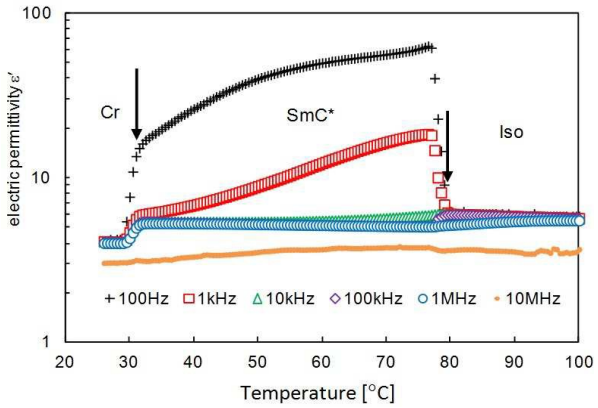

Figure 4. The real part ε' of the electric permittivity as a function of temperature (T) for compound 3FO5C2 measured at cooling for 100Hz, 1, 10, 100kHz, 1MHz and 10MHz. Arrows indicate the phase transitions.

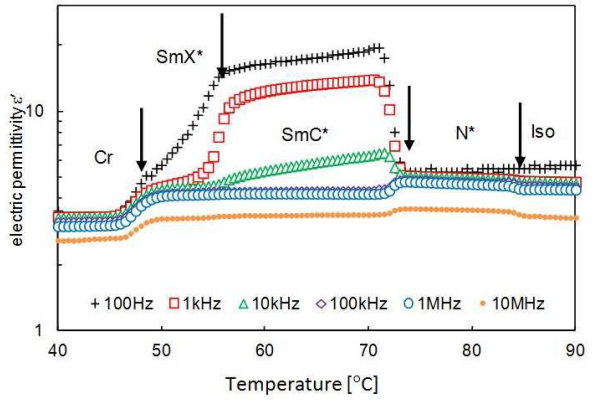

Figure 5. The real part ε' of the dielectric permittivity as a function of temperature for compound 3HO3C1 measured at cooling for 100Hz, 1, 10, 100kHz, 1MHz and 10MHz. Arrows indicate the phase transitions.

3.3 Tilt angle measurements

The tilt angle was studied by standard method[56] using custom made cells with bookshelf-like structure of the liquid crystal at the SmC* phase. Cells with the thickness of 1.5μm with ITO electrodes were coated with polyamide nylon 6.6 to obtain a homogenic alignment layer. Aligning layers have been deposited from a 0.5% solution of the dry mass in threefluoroethanol by spinning. After the drying and baking processes cells substrates with the polyamide orienting layers have been rubbed unidirectionally and assembled using a rod-like spacer in the sealing frame only. Cells have been filled with an investigated compound by capillary action at the elevated temperature enough to keep the material under study at the isotropic phase. The homogenous texture with the planar alignment of the director at smectic layers has been obtained upon a slow (0.01°C/min) cooling. The tilt angle θ upon the temperature domain has been observed during the cooling cycle at the presence of an electric field (E=2.8V/μm; f=15Hz) of magnitude enough to saturate the switching angle. The transmitted light intensity upon the angle between the direction of the smectic layer normal and the orientation of the polarizer for both electric field polarizations has been observed. The tilt angle has been obtained as half of the angle between the two minima of the light transmissions for both of the polarizations of the electric field applied.

In Figure 6 the values of the tilt angles θ as a function of temperature for compounds: 3FO6C1, 3FO7C2 and 3HO3C1 measured in the SmC* phase have been presented. The maximum of the optical tilt angle 44.9° has been observed at 106°C for compound 3FO6C1, 45.0° at 40°C for compound 3FO7C2 and 42.9° at 61°C for compound 3HO3C1. The values of the tilt angle in the all investigated compounds depend on the temperature slightly at the some distance from the Iso-SmC* transition and increase with the temperature decrease.

3.4 Spontaneous polarization measurements

The values of the spontaneous polarization (P_S) have been studied by reverse current method[57-58] using a triangle pulse of the AC electric field. The cells with the cell gap of 3.0μm have been prepared at similar way as for the tilt angle measurements. The samples have been slowly (0.1°C/min) cooled from the isotropic phase at the presence of the electric field (E=2.8V/μm; f=15Hz). The values of the P_S were obtained from the integration of the polarization reversal current peaks registered in response to the application of the voltage pulse of a triangle shape.

In Figure 7 the results of the polarization measurements upon the temperature of the SmC* phase for compounds: 3FO6C1, 3FO7C2 and 3HO3C1 has been shown. The values of the spontaneous polarization for investigated compounds are relatively high: 89.5nC/cm^2 at 101°C for compound 3FO6C1, 91.4nC/cm^2 at 40°C for compound 3FO7C2 and 103.1nC/cm^2 at 59°C for compound 3HO3C1. The values of the spontaneous polarization of all investigated compounds increase with the temperature decrease. The compound with butoxypropoxy achiral chain (3HO3C1) has the highest value of spontaneous polarization. The same relation was observed in the recently investigated benzoates with alkanoyloxyalkoxy and perfluoroalkanoyloxyalkoxy achiral chain[43-44]. For 4-octyl-2-oxycarbonylobiphenylyl-4-yl 4-(alkanoyloxy-alkoxy) benzoates and perfluoroalkanoyloxyalkoxy benzoates the opposite relation was observed. The fluorinated compounds exhibit higher P_S values.

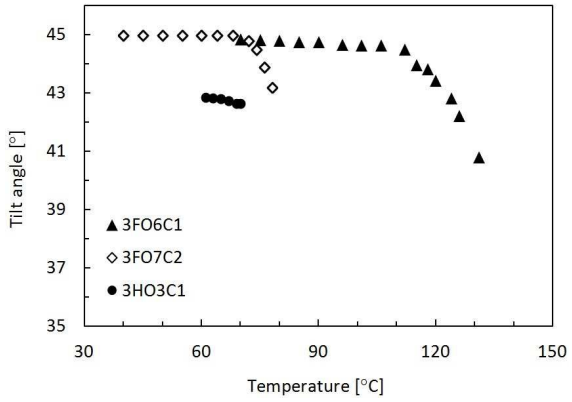

Figure 6. The tilt angle θ as a function of temperature for compounds: 3FO6C1, 3FO7C2 and 3HO3C1 measured during cooling.

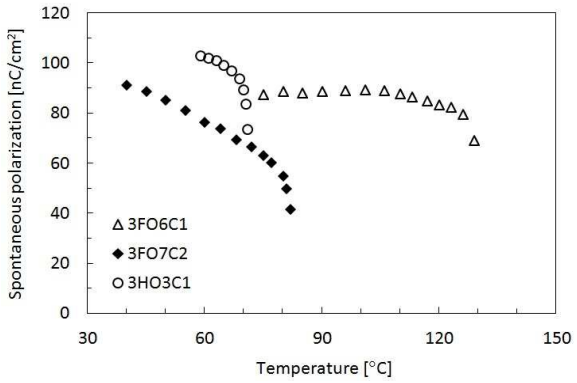

Figure 7. Spontaneous polarization P_S as a function of temperature for compounds: 3FO6C1, 3FO7C2 and 3HO3C1 measured during cooling.

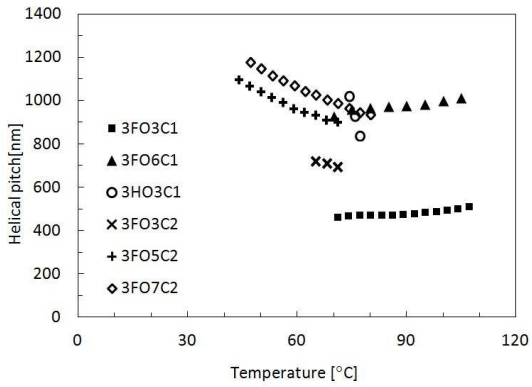

Figure 8. The length of the helical pitch vs. temperature calculated for compounds: 3FO3C1, 3FO6C1, 3HO3C1, 3FO3C2, 3FO5C2 and 3FO7C2 in the SmC*phase measured during cooling.

3.5 Helical pitch measurements

The helical pitch measurements have been done based on the selective light reflection phenomenon[59-60]. The wavelength of selectively reflected light has been calculated by observation of the minimum of the light transmission measured by a UV-VIS-NIR 3600 Shimadzu spectrophotometer in the range of 360-3000nm during cooling cycle. Cells were cooled from the isotropic phase and the temperature was controlled using the Linkam S-1700 temperature controller. The maximum of the selective reflection of the light in the SmC* phase for compounds: 3FO3C1, 3FO6C1, 3HO3C1, 3FO3C2, 3FO5C2 and 3FO7C2 was measured. The helical pitch in measured compounds was calculated using the equation: $\lambda_{max} = \check{n} \cdot p$, where λ_{max} is the length of the selectively reflected light and $\check{n}$ is the average refractive index (for the investigated compound $\check{n}$ is about 1.5[61]). The glass plate, covered by a thin layer of an investigated compound, was placed into the spectrophotometer on the way of the light ray at the side. The selective reflection was registered every 1°C. The calculated lengths of the helical pitches for measured compounds are shown in Figure 8.

The length of the helical pitch in compounds 3FO3C1 and 3FO6C1 in the SmC* phase decreases with the temperature decrease from 510.7nm at 107°C to 460.7nm at 71°C and from 1009nm at 105°C to 927 nm at 70°C respectively. For compounds: 3HO3C1, 3FO3C2, 3FO5C2 and 3FO7C2 the length of the helical pitch decreases with the temperature increase: from 1024.7nm 74°C to 840nm at 77°C, from 693.3nm 71°C to 720nm at 65°C, from 1096.7nm 44°C to 902nm at 71°C and from 1367.7nm 35°C to 938nm at 80°C respectively. For compounds 3HO3C1 the wavelength of the selective reflection in the SmC* phase below 74°C is out of the range of the spectrometer. The helical pitch p depends on the length of the oligomethylene spacer and decreases with the decrease of the index m.

4 Discussion and conclusions

The prepared compounds with fluorinated 2,2,3,3,4,4,4-heptafluorobutoxy unit in the achiral chain of both homologous series: 3FOmC1 and 3FOmC2 exhibit Cr-SmC*-Iso phase sequence and their clearing points decrease with the increasing of the m index in the oligomethylene spacer of the terminal achiral chain. The compound with butoxypropoxy chain 3HOmC1 exhibits the Cr-SmC*-N*-Iso phase sequence, similar as the alkoxy compounds obtained by Inukai, while compound 3HO3C2 with the longer branch at the chiral centre has no mesophase. Compound 3FO7C2 exhibits the widest temperature range of the synclinic, high tilted SmC* phase. The members of the homologous series 3FOmC2, having octan-3-yloxy chiral moiety, exhibit much lower melting points that compounds of the series 3FOmC1, having octan-2-yloxy chiral moiety. Changing the chiral part from oct-2-yloxy- to oct-3-yloxy- decreases the melting as well as clearing points significantly. Replacing the partially fluorinated butoxy unit in the terminal achiral chain in compounds 3FOmCk by butoxy unit (compounds 3HOmCk) destabilizes the SmC* phase. The comparison of the temperatures range of mesophases of both series 3XOmC1 and 3XOmC2 are presented in Figure 9. For compounds 3HO3C1 and 3FO3C2 the temperatures range of the phase only during cooling are given.

The Goldstone mode is detected in the ferroelectric SmC* phases. Fluorinated compounds have higher dielectric strength ($\delta\varepsilon$) of the Goldstone mode than the protonated ones and the relaxation frequency (f_R) of the Goldstone mode is lower for fluorinated compounds than for the protonated ones. The observed maximum optical tilt angle for fluorinated compounds are high: 44.9° for compound 3FO6C1 and 45.0° for compound 3FO6C1. The observed maximum optical tilt angle for protonated compound 3HO3C1 is a little bit lower, and is about 42.9°. The values of the spontaneous polarization for all investigated compounds is relatively high, above 89.5nC/cm^2. The length of the helical pitch decrease with the decrease of the m index and is the shortest for compound 3FO3C1 (460.7nm at 71°C).

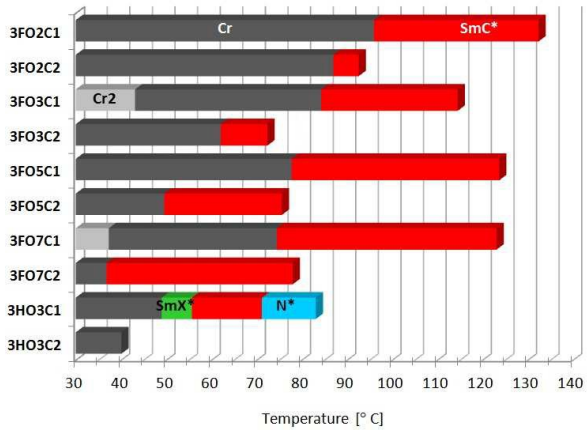

Figure 9. The comparison of the temperatures range of phases in both series 3XOmC1 and 3XOmC2.

Analogous series with an ester group in the terminal achiral chain[44-45] (marked as 3XOOmC1, see Figures 10 and 11) exhibit similar or a little lower melting points and similar phase sequence: Cr-SmC*-Iso. Also similar phase sequence show compounds 3HO3C1 and 3HOO3C1. The fluorinated compounds with the ester group in achiral chain (nFOOmC1) exhibits low-tilted SmC* phase (the tilt angle value below 20°), while fluorinated compounds 3FOmC1 has very high tilt: 45°. The tilt angle of protonated compounds (nHOOmC1) is quite high, for example: 40.3° at 60°C for compound 3HOO3C1, but lower than for compound 3HO3C1 (42.9° at 61°C). Both protonated families of compounds (3HO3C1 and 3HOO3C1) have an additional N* phase and a more ordered chiral smectic phase below SmC* phase. The replacement of the partially fluorinated terminal butoxy unit by the butoxy unit in the achiral terminal chain led to the decreasing of the stability of the SmC* phase, similar to that observed for many other liquid crystals. The length of the helical pitch in compounds nFOOmC1 is similar than in compound 3FOmC1. The length of the helical pitch in compounds nHOOmC1 is shorter than in compound 3HOmC1.

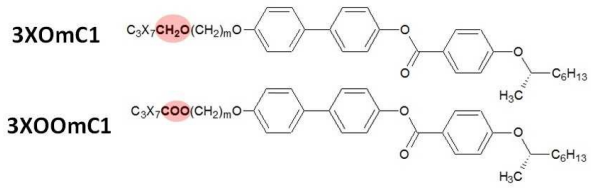

Figure 10. The structures of the series 3XOmC1 and 3XOOmC1; X=F or H.

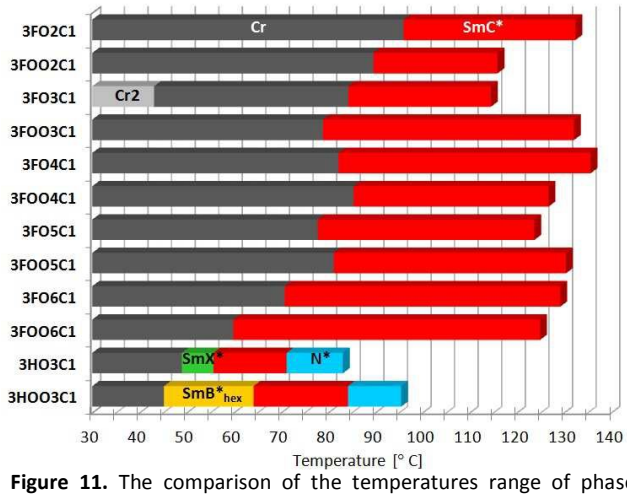

Figure 11. The comparison of the temperatures range of phase sequence of both series 3XOmC1 and 3XOOmC1.

Acknowledgements

This work has been supported by the Polish Ministry of Science and Higher Education, grant RMN No. 974/2014 and POIG.01.03.01-14-016/08. We are thankful to Mr. Edwin Myka for his help in the preparing of compounds 3FOmC2.

References

1 N. A. Clark and S. T. Lagerwall, *Appl. Phys. Lett.*, 1980, **36**, 899-901.
2 A. D. L. Chandani, A. Fukuda, S. Kumar and J. Vij, *Liq. Cryst.*, 2011, **38**, 663-668.
3 A. Bubnov, V. Novotná, D. Pociecha, V. Hamplová and M. Kašpar M, *Phase Transitions*, 2012, **85**, 849-860
4 M. Koden, Ferroelectrics, 1996, 179, 121-129.
5 V. Novotná, V. Hamplová, M. Kašpar, N. Podoliak, A. Bubnov, M. Glogarová, D. Nonnenmacher and F. Giesselmann, *Liq. Cryst.*, 2011, **38**, 649-655
6 P. Malik, K. K. Raina, A. Bubnov, A. Chaudhary and R. Singh, *Thin Solid Films*, 2010, 519, 1052-1055.
7 M. Garić, A. Bubnov, V. Novotná, M. Kašpar, V. Hamplová, D. Ž. Obadović and M. Glogarová, *Liq. Cryst.*, 2005, **32**, 565-572.
8 M. Stojanović, A. Bubnov, D. Ž. Obadović, V. Hamplová, M. Kašpar and M. Cvetinov, *Phase Transitions.*, 2011, **84**, 380-390.
9 K. Kurp, M. Czerwiński, M. Tykarska, *Liq. Cryst.*, 2015, **42**, 248-254.
10 S. Kawamoto, M. Oh-kochi, S. Kundu, H. Hasebe, H. Takatsu, S. Kobayashi, *Displays*, **25**, 45 (2004)
11 A. Fukuda, Proc. Asia Display, Hamamatsu, 95, 61 (1995)
12 T. Fujisawa, M. Hayashi, H. Hasebe, K. Takeuchi, H. Takatsu, S. Kobayashi, *DIC Technical Review*, 2007, **13**
13 E. Pozhidaev and V. Chigrinov V, SID'10 Conference, 27-2, Seattle, Washington, USA, May, 2010.
14 A. Jakli, L. Bata and L. A. Bersnev, *Mol. Cryst. Liq. Cryst.*, 1989, **177**, 43-57.
15 A. G. H. Verhulst, G. Cnossen, J. Fünfschilling and M. Schadt, *J. SID.*, 1995, **3**, 133-138.
16 J. Fünfschilling and M. Schadt, *Jpn. J. Appl. Phys.*, 1996, 35, 5765- 5774.
17 I. Abdulhalim, *Appl. Phys. Lett.*, 2012, **101**, 141903-1-5.
18 A. D. Kiselev and V. G. Chigrinov, *Phys. Re*v. E, 2014, **90**,

042504-1-19
19 A. D. Kiselev, E. Pozhidaev, V. G. Chigrinov and H.S. Kwok, *Phoonics Lett. Pol.*, 2011, **3**, 29-31
20 V. G. Chigrinov, Liquid Crystal Devices: Physics and *Applications*, 357, Artech-House, Boston- London (1999)
21 E. Pozhidaev and V. G. Chigrinov, *SID*, **41**, 2010, 387-390
22 L. A. Baresnev, V. Chigrinov, D. I. Dergachev, E. P. Poshidaev, J. Fünfshilling and M. Schadt, *Liq. Cryst.*, 1989, **5**, 1171-1177.
23 I. Abdulhalim, *Appl. Phys. Lett.*, 2012, 101, 141903-1-5.
24 S. J. Woltman, G. D. Jay and G. P. Crawford, *Nat. Mater.*, 2007, **6**, 929-938.
25 F. Anagni, C. Bartoletti, U. Marchetti, L. Podesta and G. Sacerdoti, *IEEE T Instrum Meas.*, 1994, **43**, 475-480.
26 T. Woliński, A. Czapla, S. Ertman, M. Tefelska, A. Domański, J. Wójcik, E. Nowinowski-Kruszelnicki and R. Dąbrowski, *IEEE T Instrum Meas.*, 2008, **57**, 1796-1802.
27 Z. Brodzeli, L. Silvestri, A. Michie, Q. Guo, E. P. Pozhidaev, V. Chigrinov and F. Ladouceur, *Journal of Lightwave Techn.*, 2013, **31**, 2940-2946.
28 Z. Brodzeli, L. Silvestri, A. Michie, Q. Guo, E. P. Pozhidaev, V. Chigrinov and F. Ladouceur, *Liq. Cryst.*, 2013, **40**, 1427-1435.
29 C. C. Mao, D. J. McKnight and K. M. Johnson, *Opt. Lett.*, 1995, **20**, 342-344.
30 G. B. Cohen, R. Pogreb, K. Vinokur and D. Davidov, *Appl. Opt.*, 1997, **36**, 455-459.
31 D. V. Wick, T. Martinez, M. V. Wood, J. M. Wilkes, M. T. Gruneisen, V. A. Berenberg, M. V. Vasil'ev, A. P. Onokhov and L. A. Beresnev, *Appl. Opt.*, 1999, **38**, 3798-3803.
32 J. G. Cuennet, E. A. Vasdekis and L. De Sio, D. Psaltis, Nat. Photon., 2011, **5,** 234-238.
33 Y. V. Izdebskaya, V. G. Shvedov, A. S. Desyatnikov, W. Krolikowski and Y. S. Kivshar, *Opt. Lett.*, 2010, 35, 1692-1694.
34 Z. Ge, S. Gauza, M. Jiao, H. Xianyu and S. T. Wu, *Appl. Phys. Lett.*, 2009, **94**, 101104-3.
35 Z. Brodzeli, F. Ladouceur, L. Silvestri, A. Michie, V. Chigrinov, Q. Guo, E. P. Pozhidaev and A. D. Kiselev, *Third Asia Pacific Optical Sensors Conference*, 2012, 83512C.
36 Z. Brodzeli, L. Silvestri, A. Michie, V. Chigrinov, Q. Guo, E. P. Pozhidaev, A. D. Kiselev and F. Ladouceur F, *Photonic Sensors*, 2012, **2**, 237246.
37 A. Nafees, G. Kalita, M. K. Paul, A. Sinha and N. V. S. Rao, *RSC Advances*, 2015, **5**, 7001-7006.
38 S. Ghosh, N. Begum, S. Turlapati, S. K. Roy, A. K. Das and N. V. S. Rao, *J. Mater. Chem.* C, 2014, **2**, 425-431.
39 M. Hird, Liq. Cryst., 2011, **38**, 1467-1493.
40 P. Kula, J. Herman and O. Chojnowska, *Liq. Cryst.*, 2013, **40**, 83-90.
41 M. Czerwiński, M. Tykarska, R. Dąbrowski, A. Chełstowska, M. Żurowska, R. Kowerdziej and L. R. Jaroszewicz, *Liq. Cryst.*, 2012, **39**, 1498-1502.
42 T. Inukai, S. Saitoh, H. Inoue, K. Miyzawa, K. Terashima and K. Furukawa, *Mol. Cryst. Liq. Cryst.*, 1986, **141**, 251-266.
43 C. T. Liao, J. Y. Lee and C. C. Lai, *Mol. Cryst. Liq. Cryst.*, 2011, **534**, 95-113.
44 D. Ziobro, R. Dąbrowski, M. Tykarska, W. Drzewiński, M. Filipowicz, W. Rejmer, K. Kuśmierek, P. Morawiak and W. Piecek, *Liq. Cryst.*, 2012, **39**, 1011–1032.
45 D. Węgłowska and R. Dąbrowski, *Liq. Cryst.*, 2014, **41**, 1116-1129.
46 E. Myka, M. Sc. Thesis. Military University of Technology, 2015.
47 O. Mitsunobu and M. Yamada, *Bull. Chem. Soc. Jpn.*, 1967, **40**, 2380-2382.
48 P. Kula, A. Spadło, M. Żurowska and R. Dąbrowski, *Synlett.*, 2010, **9**, 1394-1396.
49 D. Demus, JW Goodby, GW Gray, HW Spiess and V. Vill , *Handbook of liquid crystals. Low molecular weight liquid crystals I. Vol. 2A.* Weinheim: Wiley-VCH; 1998. pp. 530.
50 M. Mrukiewicz, P. Perkowski and K. Garbat, Liquid Crystals. 2015, DOI: 10.1080/02678292.2015.1020893
51 P. Perkowski, *Opto-Electron Rev.*, 2009, **17**, 180-186.
52 S. T. Lagerwall, *Ferroelectric and Antiferroelectric Liquid Crystals*, Wiley-Vch, Weinheim 1999
53 P. Perkowski, *Opto-Electronics Rev.*, 2009, **17**, 180-186.
54 P. Perkowski, *Opto-Electronics Rev.*, 2011, **19**, 176-182.
55 M. Mrukiewicz, P. Perkowski, K. Garbat and R. Dąbrowski, *Liq. Cryst.*, 2014, **41**, 1537-1544.
56 W. Piecek, Z. Raszewski, P. Perkowski, J. Kędzierski, J. Rutkowska, E. Nowinowski-Kruszelnicki, J. Zielinski, R. Dąbrowski and X. W. Sun, *Mol. Cryst. Liq. Cryst.*, 2007, **477**, 205-221.
57 J. Gąsowska, R. Dąbrowski, W. Drzewiński, M. Filipowicz, J. Przedmojski and K. Kenig, *Ferroelectrics*, 2004, **309**, 83-93.
58 R. Dąbrowski, J. Gąsowska, J. Oton, W. Piecek, J. Przedmojski and M. Tykarska, *Displays*, 2004, **25**, 9-19.
59 M. Tykarska, M. Czerwiński and J. Miszkurka, *Liq. Cryst.*, 2010, **37**, 487-495.
60 A. Chełstowska, M. Czerwiński, M. Tykarska, N. Bennis, L*iq. Cryst.*, 2014, **41**, 812–820.
61 Z. Raszewski, J. Kędzierski, P. Perkowski, W. Piecek, J. Rutkowska, S. Kłosowicz, J. Zieliński, Ferroelectrics, 2002, 276, 289-290.